Int. J Heat Mass Transfer. Vol. 35, No. 4, pp. 897–912, 1992
Printed in Great Britain

0017–9310/92 $5.00 + 0.00

Propagation and reflection of thermal waves in a finite medium due to axisymmetric surface sources

LOUIS G. HECTOR, JR.
Product Manufacturing Technology Division, Alcoa Laboratories, Alcoa Center, PA 15069, U.S.A.

WOO-SEUNG KIM
Department of Mechanical Engineering, Hanyang University, Seoul 133, Korea

and

M. N. ÖZISIK
Department of Mechanical and Aerospace Engineering, North Carolina State University, Raleigh, NC 27695, U.S.A.

(*Received* 1 *October* 1990 *and in final form* 20 *March* 1991)

Abstract—For situations involving extremely short times following the start of transients, or very high heat fluxes, the classical diffusion theory of heat conduction breaks down since the wave nature of thermal energy transport dominates. In this work, the hyperbolic temperature response in a finite, isotropic medium with one surface insulated and the other surface irradiated with an axially symmetric heat flux is considered. The spatial profile of the heat flux is chosen to be either Gaussian, doughnut-shaped, or some combination of the two. The temporal profile is either continuous or a rectangular pulse. The choice of these profiles is based upon the premise that they approximate the outputs from some common laser sources. Calculations for a Gaussian source reveal the existence of a severe thermal wavefront which propagates through the medium, dissipating energy in its wake upon reflection at the boundaries. Also discussed is the relative importance of the parabolic and hyperbolic heat conduction models for a metal exposed to three ranges of rectangular pulse duration.

INTRODUCTION

In Fourier heat conduction, the constitutive law which relates heat flux $\mathbf{q}$ to the temperature gradient ∇T is of the form

$$\mathbf{q}(\bar{r}, t) = -k\nabla T \tag{1}$$

where k is the thermal conductivity. While the heat conduction equation based on this model is acceptable for the majority of practical situations, it fails to adequately predict temperatures in situations involving extremely short periods of time, extreme temperature gradients, or very low temperatures. To avoid difficulties in such situations, the following hyperbolic constitutive law, which accounts for a finite build-up time for the flow of heat, has been proposed:

$$\tau\frac{\partial \mathbf{q}}{\partial t} + \mathbf{q} = -k\nabla T. \tag{2}$$

Equation (2), which is actually a truncated version of a more general relation originally derived by Maxwell [1] during the course of his work on the kinetic theory of gases, states that heat flow does not begin immediately following a thermal disturbance, but in fact grows with the relaxation time τ. The relaxation time is a measure of the thermal inertia of the medium in much the same way that the ratio of inductance to electrical resistance is a measure of electrical inertia in a transmission line [2], for example. A typical value of the relaxation time τ for metals has been reported [3] to be of the order of 10^{-11} s, while recent work by Kaminsky [4] on non-homogeneous inner structure materials revealed values of τ of the order of fractions of a minute. When equation (2) is combined with the energy equation, the following heat conduction equation results:

NOMENCLATURE

A fraction of surface heat flux containing Gaussian mode
c speed of thermal wave propagation
C_p specific heat
d characteristic beam radius
$f(t)$ temporal profile of surface heat flux [dimensionless]
$f_i(\eta; m)$ functions defined by equations (24b) and (24c)
$F(\xi)$ dimensionless temporal profile of surface heat flux
$g(\beta)$ defined by equation (19)
$G_1(\rho, \eta, \xi)$ function defined by equation (28b)
$G_2(\rho, \eta, \xi)$ function defined by equation (32b)
$G_3(\rho, \eta, \xi)$ function defined by equation (C2)
$G_4(\rho, \eta, \xi)$ function defined by equation (C3)
$H(\xi)$ unit step function of argument ξ
$I_0(x)$ modified Bessel function of the first kind of order zero
$J_0(x)$ Bessel function of the first kind of order zero
k thermal conductivity
L medium thickness
m summation index
$q(r, z, t)$ heat flux
q_0 scaling factor
Δq_ℓ limiting heat flux
r radial space variable
s Laplace transform variable
t time variable
Δt temporal pulse width
$T(r, z, t)$ temperature
T_0 base temperature
z axial space variable.

Greek symbols
α thermal diffusivity
β transform variable
γ attenuation coefficient
Γ defined by equation (A6)
$\delta(\xi)$ delta function of argument ξ
η dimensionless axial space variable
η_ℓ dimensionless medium thickness
$\theta(\rho, \eta, \xi)$ dimensionless temperature
$\bar{\theta}(\rho, \eta, \xi)$ first transform of dimensionless temperature
$\tilde{\bar{\theta}}(\rho, \eta, \xi)$ second transform of dimensionless temperature
μ dimensionless reciprocal of characteristic beam radius
ρ dimensionless radial space variable
$\bar{\rho}$ density
ξ dimensionless time variable
ξ^* defined by equation (36b)
$\Delta\xi$ dimensionless temporal pulse width
ω dimensionless parameter defined by equation (22b).

Subscripts
ℓ dimensionless medium thickness or limiting heat flux
p specific heat
r radial heat flux component
z axial heat flux component
1, 2, 3, 4 functions defined by equations (28b), (32b), (C2), and (C3).

$$\nabla^2 T = \frac{1}{c^2}\frac{\partial^2 T}{\partial t^2} + \frac{1}{\alpha}\frac{\partial T}{\partial t} \tag{3}$$

where constant properties have been assumed for a medium with no energy generation. This equation, which is hyperbolic in nature, reduces to the standard parabolic heat conduction equation as the speed of energy propagation, c, becomes infinite. Corrections to equation (3) which involve higher order time and space derivatives on temperature have been derived by Simons [5].

Although equation (2) was originally derived in the framework of an ideal gas, Chester [6] has suggested that it should apply equally well to solids which may be considered as phonon gases in which an individual phonon represents a mechanical vibration of atoms. Hence, a thermal wave propagates through a solid as a phonon density disturbance. When a solid is irradiated with a laser of sufficient power over very short intervals for example, such a disturbance results when the absorbed photon energy from the beam is converted into kinetic energy of free electrons, which is then transferred to the lattice atoms [7].

The wave nature of heat propagation has been the subject of numerous investigations. For example, Carey and Tsai [8] used the finite element method to solve the hyperbolic heat conduction equation in a finite medium for two sets of boundary conditions. Özisik and Vick [9] considered hyperbolic heat conduction in a medium with insulated boundaries subjected to a volumetric energy source in the form of a concentrated pulse of energy. Their analysis was thus appropriate for a material which is a good absorber of heat. The energy pulse was found to give rise to a severe thermal wavefront which dissipated energy in its wake as it traveled from the front to the rear boundary of the medium. Upon striking the rear boundary, the wave reversed its direction

of propagation and continued to dissipate its energy on its trip back to the front boundary. Frankel *et al.* [10] developed a flux formulation for hyperbolic heat conduction and again considered traveling thermal waves due to a pulse of energy within a finite medium. Interest in the temperature response due to impulsive mechanical loading of a linear elastic material has given rise to a considerable body of literature dealing with the simultaneous propagation of coupled thermal and mechanical waves through the material [11].

The existing hyperbolic heat conduction analyses consider only unidimensional heat conduction. For situations which involve laser beam irradiation of a surface, it is appropriate to consider the spatial profile of the impinging beam in a heat conduction analysis. For example, most pulsed solid state lasers will operate in the lowest order spatial mode which is known as TEM_{00}† or Gaussian mode. Many high power CO_2 and solid state lasers operating in an industrial environment emit beams which are generally complicated mixtures of the two lowest order spatial modes [12], TEM_{00} and TEM_{01^*}, the latter mode of which is often referred to as the doughnut mode. These spatial distributions are generally axisymmetric although in practice some deviation from axial symmetry is usually inevitable due to the type of resonator used, imperfections in the laser medium, and thermal effects. The spatial profile of the beam influences the extent of the heat affected zone and the degree to which material on, and adjacent to the surface is metallurgically altered [13].

Several authors [14–16] have studied the effects of axisymmetric sources using the parabolic heat conduction equation. However, the results of such analyses are not always applicable to situations involving extremely short pulses, such as those which are emitted by various solid state lasers, for which the pulse widths can be in the nanosecond–picosecond range, and the high initial heat fluxes involved in certain surface engineering processes [17].

The use of a surface source in a heat conduction analysis associated with laser irradiation is based on the fact that a laser beam which irradiates a metal surface is absorbed in a thin layer which is generally several hundred ångströms in thickness. According to Sparks [18], the absorbing layer is sufficiently thin so as to warrant the assumption that the incident radiation may be considered a surface source. This situation corresponds to a material for which the optical attenuation coefficient is large. For a typical metal, the attenuation coefficient falls in the range of 10^5–10^6 cm^{-1} [19].

The present work is concerned with the investigation of the temperature response in a finite region to axisymmetric surface sources which are either temporally continuous or rectangular pulses activated for a small period Δt. The spatial profile of the source may be either Gaussian, doughnut or mixed, the latter being a combination of the Gaussian and doughnut modes. The material properties are assumed constant, and radiation and convection from the irradiated surface are neglected. Appendix A of this paper contains a discussion of the relative importance of the hyperbolic and parabolic heat conduction models for a metal irradiated with three ranges of pulse width from a solid state laser. The purpose of this appendix is to outline one realm of practical application of hyperbolic heat conduction.

PROBLEM FORMULATION

The energy conservation equation in cylindrical coordinates is given by

$$\frac{1}{r}\frac{\partial}{\partial r}(rq_r)+\frac{\partial q_z}{\partial z}-\bar{\rho}C_p\frac{\partial T}{\partial t}=0 \tag{4}$$

where q_r and q_z are the radial and axial components of the heat flux vector, respectively. The hyperbolic constitutive equations, which are valid at all points in the medium, are written as

$$\tau\frac{\partial q_r}{\partial t}+q_r=-k\frac{\partial T}{\partial r} \tag{5}$$

$$\tau\frac{\partial q_z}{\partial t}+q_z=-k\frac{\partial T}{\partial z}. \tag{6}$$

When the heat flux components are eliminated from equations (4) to (6), the following hyperbolic heat conduction equation which governs the temperature distribution in an isotropic medium which has no volumetric energy sources results:

$$\frac{\partial^2 T}{\partial r^2}+\frac{1}{r}\frac{\partial T}{\partial r}+\frac{\partial^2 T}{\partial z^2}=\frac{1}{\alpha}\frac{\partial T}{\partial t}+\frac{1}{c^2}\frac{\partial^2 T}{\partial t^2},\quad \text{in}\quad r>0, 0<z<L, t>0 \tag{7}$$

where c is the speed of the thermal wavefront which is related to the relaxation time τ through

† TEM: transverse electric and magnetic mode.

$$c^2 = \frac{\alpha}{\tau}. \tag{8}$$

The classical heat conduction equation which corresponds to instantaneous energy diffusion is retrieved when $\tau \to 0$. Note that absorption of laser irradiation can be modeled as a volumetric heat source and this is briefly discussed in Appendix B as it relates to the problems addressed in this work.

The present investigation is concerned with axisymmetric, two-dimensional heat conduction in a medium with constant thermal properties and no energy generation. For times $t > 0$, the surface $z = 0$ is irradiated by a source with specified spatial and temporal profiles, while the surface $z = L$ is kept insulated and will thus reflect the thermal wave incident to it. The initial conditions are thus

$$T = T_0, \quad \text{for} \quad t = 0 \tag{9a}$$

$$\frac{\partial T}{\partial t} = 0, \quad \text{for} \quad t = 0. \tag{9b}$$

The surface heat flux [20] is specified as

$$q_z = q_0 f(t)\left[A + (1-A)\frac{r^2}{d^2}\right] e^{-(r^2/d^2)}, \quad \text{on} \quad z = 0 \tag{10a}$$

where q_0 is a factor corresponding to the maximum incident flux for a Gaussian source and contains important information about surface physics, e.g. reflectivity, etc. The parameter d is a characteristic beam radius which represents the circular boundary within the Gaussian source that contains 63% of the total beam power incident to the surface. The function $f(t)$ is the temporal profile of the heat flux which is dimensionless. The parameter A is the fraction of the total flux that contains the Gaussian mode and may be represented by

$$A = \frac{\text{TEM}_{00}}{\text{TEM}_{00} + \text{TEM}_{01^*}} \tag{10b}$$

where A falls in the range $0 \leqslant A \leqslant 1$. Figure 1(a) depicts the spatial profile given by equation (10a) for $0 < A < 1$. Figure 1(b) shows the Gaussian source which corresponds to case $A = 1$. The maximum irradiance for a Gaussian source occurs at its center and is generally the reason why it is the preferred source for many material processing applications involving highly reflective metallic surfaces. The doughnut source corresponds to the case $A = 0$ and represents a situation where the maximum irradiance is not only reduced from that of the Gaussian source but is concentrated in a ring about the center of the profile which is at zero irradiance. The doughnut source is generally useful in situations where the concentrated energy ring leads to a better edge quality in various cutting operations.

When equation (10a) is combined with equation (6) and the result evaluated at $z = 0$, the following boundary condition on temperature results:

$$-k\frac{\partial T}{\partial z} = q_0\left[f(t) + \tau\frac{\mathrm{d}f(t)}{\mathrm{d}t}\right]\left[A + (1-A)\frac{r^2}{d^2}\right] e^{-(r^2/d^2)}, \quad \text{on} \quad z = 0. \tag{11}$$

Additional boundary conditions on temperature are

$$T \to T_0, \quad \text{as} \quad r \to \infty \tag{12a}$$

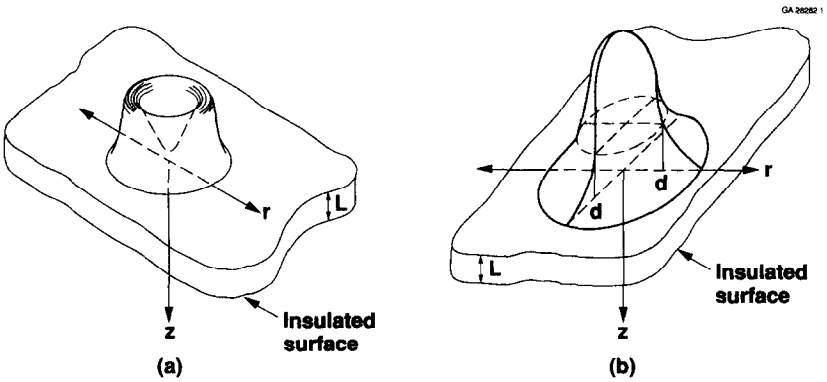

FIG. 1. Spatial profiles of laser sources: (a) doughnut; (b) Gaussian.

$$\frac{\partial T}{\partial r} = 0, \quad \text{on} \quad r = 0 \tag{12b}$$

$$\frac{\partial T}{\partial z} = 0, \quad \text{on} \quad z = L. \tag{12c}$$

For convenience in the subsequent analysis, we introduce the following dimensionless quantities:

$$\rho = \frac{cr}{2\alpha}, \quad \text{the dimensionless radial distance} \tag{13a}$$

$$\eta = \frac{cz}{2\alpha}, \quad \text{the dimensionless axial distance} \tag{13b}$$

$$\eta_\ell = \frac{cL}{2\alpha}, \quad \text{the dimensionless thickness} \tag{13c}$$

$$\xi = \frac{c^2 t}{2\alpha}, \quad \text{the dimensionless time} \tag{13d}$$

$$\mu = \frac{2\alpha}{cd}, \quad \text{the dimensionless reciprocal of } d \tag{13e}$$

$$\theta(\rho, \eta, \xi) = \frac{T(r, z, t) - T_0}{q_0 \alpha / kc}, \quad \text{the dimensionless temperature.} \tag{13f}$$

The temperature problem defined by energy equation (7) along with equations (9a), (9b), (11) and (12a)–(12c) is expressed in dimensionless form as

$$\frac{\partial^2 \theta}{\partial \rho^2} + \frac{1}{\rho}\frac{\partial \theta}{\partial \rho} + \frac{\partial^2 \theta}{\partial \eta^2} = 2\frac{\partial \theta}{\partial \xi} + \frac{\partial^2 \theta}{\partial \xi^2}, \quad \text{in} \quad \rho > 0, 0 < \eta < \eta_\ell, \xi > 0 \tag{14a}$$

$$\theta = 0, \quad \text{for} \quad \xi = 0 \tag{14b}$$

$$\frac{\partial \theta}{\partial \xi} = 0, \quad \text{for} \quad \xi = 0 \tag{14c}$$

$$\frac{\partial \theta}{\partial \eta} = -2F(\xi)[A + (1-A)\mu^2\rho^2]\,\mathrm{e}^{-\mu^2\rho^2}, \quad \text{on} \quad \eta = 0 \tag{14d}$$

$$\frac{\partial \theta}{\partial \eta} = 0, \quad \text{on} \quad \eta = \eta_\ell \tag{14e}$$

$$\theta \to 0, \quad \text{as} \quad \rho \to \infty \tag{14f}$$

$$\frac{\partial \theta}{\partial \rho} = 0, \quad \text{on} \quad \rho = 0 \tag{14g}$$

where the function $F(\xi)$ represents the dimensionless temporal profile of the surface heat flux. Solutions of this system for prescribed $F(\xi)$ and A are presented in the following sections.

ANALYSIS

The solution of the hyperbolic system (14) is examined below for a continuous Gaussian source, a continuous doughnut source, a continuous mixed source, a single pulse Gaussian source, a single pulse doughnut source, and a single pulse mixed source. The solutions for the corresponding parabolic (i.e. Fourier) system are listed in Appendix C for purposes of comparison with the hyperbolic solutions.

Continuous Gaussian source

For a continuous Gaussian source, $f(t) = H(t)$ and $A = 1$. The dimensionless form of equation (11) becomes

$$\frac{\partial \theta}{\partial \eta} = -[2H(\xi) + \delta(\xi)]\,\mathrm{e}^{-\mu^2\rho^2}, \quad \text{on} \quad \eta = 0. \tag{15}$$

In order to solve equation (14a) subject to equations (14b), (14c), (14e)–(14g) and (15), the following integral transform pair on the ρ-variable is introduced:

transform

$$\bar{\theta}(\beta,\eta,\xi)=\int_{\rho'=0}^{\infty}\rho' J_0(\beta\rho')\theta(\rho',\eta,\xi)\,\mathrm{d}\rho' \tag{16a}$$

inversion

$$\theta(\rho,\eta,\xi)=\int_{\beta=0}^{\infty}\beta J_0(\beta\rho)\bar{\theta}(\beta,\eta,\xi)\,\mathrm{d}\beta \tag{16b}$$

where $J_0(x)$ is the zero-order Bessel function of the first kind. In order to transform system (14), we operate on these equations with

$$\int_{\rho'=0}^{\infty}\rho' J_0(\beta\rho')\,\mathrm{d}\rho' \tag{17}$$

which gives

$$\frac{\partial^2\bar{\theta}}{\partial\eta^2}=2\frac{\partial\bar{\theta}}{\partial\xi}+\frac{\partial^2\bar{\theta}}{\partial\xi^2}+\beta^2\bar{\theta},\quad\text{in}\quad 0<\eta<\eta_f,\ \xi>0 \tag{18a}$$

$$\bar{\theta}=0,\quad\text{for}\quad\xi=0 \tag{18b}$$

$$\frac{\partial\bar{\theta}}{\partial\xi}=0,\quad\text{for}\quad\xi=0 \tag{18c}$$

$$\frac{\partial\bar{\theta}}{\partial\eta}=-[2H(\xi)+\delta(\xi)]g(\beta),\quad\text{on}\quad\eta=0 \tag{18d}$$

$$\frac{\partial\bar{\theta}}{\partial\eta}=0,\quad\text{on}\quad\eta=\eta_f \tag{18e}$$

where the function $g(\beta)$ is defined by

$$g(\beta)=\int_{\rho'=0}^{\infty}\rho'\,\mathrm{e}^{-\mu^2\rho'^2}J_0(\beta\rho')\,\mathrm{d}\rho'. \tag{19}$$

Application of the Laplace transform defined by

$$\tilde{\bar{\theta}}(\beta,\eta,s)=\int_{\xi'=0}^{\infty}\mathrm{e}^{-s\xi'}\bar{\theta}(\beta,\eta,\xi')\,\mathrm{d}\xi' \tag{20}$$

to equations (18a)–(18e), gives the following system for the double transform $\tilde{\bar{\theta}}(\beta,\eta,s)$:

$$\frac{\mathrm{d}^2\tilde{\bar{\theta}}}{\mathrm{d}\eta^2}-(\beta^2+s^2+2s)\tilde{\bar{\theta}}=0,\quad\text{in}\quad 0<\eta<\eta_f \tag{21a}$$

$$\frac{\mathrm{d}\tilde{\bar{\theta}}}{\mathrm{d}\eta}=-\left[\frac{2}{s}+1\right]g(\beta),\quad\text{on}\quad\eta=0 \tag{21b}$$

$$\frac{\mathrm{d}\tilde{\bar{\theta}}}{\mathrm{d}\eta}=0,\quad\text{on}\quad\eta=\eta_f. \tag{21c}$$

The solution to equation (21a) subject to equations (21b) and (21c) is

$$\tilde{\bar{\theta}}(\beta,\eta,s)=\frac{g(\beta)}{\omega(1-\mathrm{e}^{-2\omega\eta_f})}\left[\frac{2}{s}+1\right][\mathrm{e}^{-\omega\eta}+\mathrm{e}^{-\omega(2\eta_f-\eta)}] \tag{22a}$$

where the dimensionless parameter ω is given by

$$\omega=\sqrt{((s+1)^2+\beta^2-1)}. \tag{22b}$$

For large values of ω (or small values of t) we may write

$$\frac{1}{1-\mathrm{e}^{-2\omega\eta_f}}=\sum_{m=0}^{\infty}\mathrm{e}^{-2m\omega\eta_f} \tag{23}$$

and hence equation (22a) may be re-written as

$$\tilde{\theta}(\beta,\eta,s)=\frac{g(\beta)}{\omega}\left[\frac{2}{s}+1\right]\sum_{m=0}^{\infty}(\mathrm{e}^{-\omega f_1(\eta;m)}+\mathrm{e}^{-\omega f_2(\eta;m)}) \tag{24a}$$

where

$$f_1(\eta;m)=2m\eta_\ell+\eta \tag{24b}$$

$$f_2(\eta;m)=2m\eta_\ell+(2\eta_\ell-\eta). \tag{24c}$$

Using the Laplace transform inversion rule [21]

$$L^{-1}\left\{\frac{1}{s}\bar{h}(s\mp a)\right\}=\int_{\xi'=0}^{\xi}\mathrm{e}^{\pm a\xi'}\tilde{h}(\xi')\,\mathrm{d}\xi' \tag{25}$$

the term $\mathrm{e}^{-\omega f_i(\eta;m)}/\omega s$ in equation (24a) is inverted to

$$L^{-1}\left(\frac{\mathrm{e}^{-\omega f_i(\eta;m)}}{\omega s}\right)=\begin{cases}\displaystyle\int_{\xi'=0}^{\xi}\mathrm{e}^{-\xi'}I_0(\sqrt{(1-\beta^2)}\sqrt{(\xi'^2-f_i^2(\eta;m))})H(\xi'-f_i(\eta;m))\,\mathrm{d}\xi', & \text{for } 0\leqslant\beta\leqslant 1\\ \displaystyle\int_{\xi'=0}^{\xi}\mathrm{e}^{-\xi'}J_0(\sqrt{(\beta^2-1)}\sqrt{(\xi'^2-f_i^2(\eta;m))})H(\xi'-f_i(\eta;m))\,\mathrm{d}\xi', & \text{for } 1\leqslant\beta<\infty\end{cases} \tag{26}$$

The integral defined by equation (19) evaluates to [22]

$$g(\beta)=\frac{\mathrm{e}^{-(\beta^2/4\mu^2)}}{2\mu^2}. \tag{27}$$

Finally, the double inversion of equation (24a) gives the desired solution as

$$\theta(\rho,\eta,\xi)=\sum_{m=0}^{\infty}\left[\frac{\mathrm{e}^{-\xi}}{2}G_1(\rho,f_1(\eta;m),\xi)H(\xi-f_1(\eta;m))+\int_{\xi'=f_1(\eta;m)}^{\xi}\mathrm{e}^{-\xi'}G_1(\rho,f_1(\eta;m),\xi')\,\mathrm{d}\xi'\right.$$
$$\left.+\frac{\mathrm{e}^{-\xi}}{2}G_1(\rho,f_2(\eta;m),\xi)H(\xi-f_2(\eta;m))+\int_{\xi'=f_2(\eta;m)}^{\xi}\mathrm{e}^{-\xi'}G_1(\rho,f_2(\eta;m),\xi')\,\mathrm{d}\xi'\right] \tag{28a}$$

where

$$G_1(\rho,f_i(\eta;m),\xi)=\frac{1}{\mu^2}\left\{\int_{\beta=0}^{1}\beta\,\mathrm{e}^{-(\beta^2/4\mu^2)}J_0(\beta\rho)I_0(\sqrt{(1-\beta^2)}\sqrt{(\xi^2-f_i^2(\eta;m))})\,\mathrm{d}\beta\right.$$
$$\left.+\int_{\beta=1}^{\infty}\beta\,\mathrm{e}^{-(\beta^2/4\mu^2)}J_0(\beta\rho)J_0(\sqrt{(\beta^2-1)}\sqrt{(\xi^2-f_i^2(\eta;m))})\,\mathrm{d}\beta\right\} \tag{28b}$$

and $I_0(x)$ is the modified Bessel function of the first kind of order zero. Recalling the definitions of f_1 and f_2 given by equations (24b) and (24c), we observe that the first two terms in equation (28a) represent the thermal waves propagating from $\eta=0$ to η_ℓ. The second two terms represent the thermal waves reflected from the insulated boundary at $\eta=\eta_\ell$. The integrals in equation (28a) cannot be expressed in terms of tabulated functions and must therefore be evaluated numerically.

It is of interest to consider the limit as the finite region approaches a semi-infinite region, i.e. as $\eta_\ell\to\infty$. The limit of equations (28a) is

$$\lim_{\eta_\ell\to\infty}[\theta(\rho,\eta,\xi)]=\frac{\mathrm{e}^{-\xi}}{2}G_1(\rho,\eta,\xi)H(\xi-\eta)+\int_{\xi'=\eta}^{\xi}\mathrm{e}^{-\xi'}G_1(\rho,\eta,\xi')\,\mathrm{d}\xi' \tag{29a}$$

where

$$G_1(\rho,\eta,\xi)=\frac{1}{\mu^2}\left\{\int_{\beta=0}^{1}\beta\,\mathrm{e}^{-(\beta^2/4\mu^2)}J_0(\beta\rho)I_0(\sqrt{(1-\beta^2)}\sqrt{(\xi^2-\eta^2)})\,\mathrm{d}\beta\right.$$
$$\left.+\int_{\beta=1}^{\infty}\beta\,\mathrm{e}^{-(\beta^2/4\mu^2)}J_0(\beta\rho)J_0(\sqrt{(\beta^2-1)}\sqrt{(\xi^2-\eta^2)})\,\mathrm{d}\beta\right\}. \tag{29b}$$

Equations (28a) and (29a) predict the same temperature distribution in the medium prior to the time when the thermal wavefront reflects from the insulated boundary at $\eta=\eta_\ell$. The first term in equation (29a) has a purely dissipative wave nature which becomes vanishingly small at longer times. The second term in equation (29a) is a correction to the thermal field which results from both the dissipative wave nature and the diffusive

nature of the problem in that it is inactive for the time period $\xi < \eta$ and eventually reduces to the solution to the Fourier heat conduction equation at longer times (see Appendix C). The second term effectively 'smears' the dissipative wave behavior of the thermal field into diffusive behavior, with time.

Continuous doughnut source

The doughnut source depicted in Fig. 1(a) is characterized by a central irradiance minimum, which corresponds to zero heat flux, surrounded by a concentrated ring of energy. In this case, $f(t) = H(t)$, $A = 0$, and the dimensionless form of equation (11) becomes

$$\frac{\partial\theta}{\partial\eta} = -[2H(\xi)+\delta(\xi)]\mu^2\rho^2\,\mathrm{e}^{-\mu^2\rho^2}, \quad \text{on} \quad \eta = 0. \tag{30}$$

A comparison of equations (15) and (30) reveals that the flux due to the doughnut source is a higher order radial distribution of energy as is evident from the $\mu^2\rho^2$ multiplier. Following the solution procedure as previously outlined for the continuous Gaussian source, with a proper interpretation of the integral [22]

$$\int_{\rho'=0}^{\infty} \rho'^3\,\mathrm{e}^{-\mu^2\rho'^2} J_0(\beta\rho')\,\mathrm{d}\rho' = \frac{1}{2\mu^4}\left(1-\frac{\beta^2}{4\mu^2}\right)\mathrm{e}^{-(\beta^2/4\mu^2)} \tag{31}$$

we find the following dimensionless temperature:

$$\theta(\rho,\eta,\xi) = \sum_{m=0}^{\infty}\left[\frac{\mathrm{e}^{-\xi}}{2}G_2(\rho,f_1(\eta;m),\xi)H(\xi-f_1(\eta;m)) + \int_{\xi'=f_1(\eta;m)}^{\xi}\mathrm{e}^{-\xi'}G_2(\rho,f_1(\eta;m),\xi')\,\mathrm{d}\xi'\right.$$
$$\left. + \frac{\mathrm{e}^{-\xi}}{2}G_2(\rho,f_2(\eta;m),\xi)H(\xi-f_2(\eta;m)) + \int_{\xi'=f_2(\eta;m)}^{\xi}\mathrm{e}^{-\xi'}G_2(\rho,f_2(\eta;m),\xi')\,\mathrm{d}\xi'\right] \tag{32a}$$

where

$$G_2(\rho,f_i(\eta;m),\xi) = \frac{1}{\mu^2}\left\{\int_{\beta=0}^{1}\beta\left(1-\frac{\beta^2}{4\mu^2}\right)\mathrm{e}^{-(\beta^2/4\mu^2)}J_0(\beta\rho)I_0(\sqrt{(1-\beta^2)}\sqrt{(\xi^2-f_i^2(n;m))})\,\mathrm{d}\beta\right.$$
$$\left. + \int_{\beta=1}^{\infty}\beta\left(1-\frac{\beta^2}{4\mu^2}\right)\mathrm{e}^{-(\beta^2/4\mu^2)}J_0(\beta\rho)J_0(\sqrt{(\beta^2-1)}\sqrt{(\xi^2-f_i^2(n;m))})\,\mathrm{d}\beta\right\}. \tag{32b}$$

Continuous mixed source

The temperature response to the continuous mixed source may be written as a combination of the solutions given by equations (28a) and (32a). This is

$$\theta(\rho,\eta,\xi) = \sum_{m=0}^{\infty}\left[\frac{\mathrm{e}^{-\xi}}{2}\{AG_1(\rho,f_1(\eta;m),\xi)+(1-A)G_2(\rho,f_1(\eta;m),\xi)\}H(\xi-f_1(\eta;m))\right.$$
$$+\int_{\xi'=f_1(\eta;m)}^{\xi}\mathrm{e}^{-\xi'}\{AG_1(\rho,f_1(\eta;m),\xi')+(1-A)G_2(\rho,f_1(\eta;m),\xi')\}\,\mathrm{d}\xi'$$
$$+\frac{\mathrm{e}^{-\xi}}{2}\{AG_1(\rho,f_2(\eta;m),\xi)+(1-A)G_2(\rho,f_2(\eta;m),\xi)\}H(\xi-f_2(\eta;m))$$
$$\left.+\int_{\xi'=f_2(\eta;m)}^{\xi}\mathrm{e}^{-\xi'}\{AG_1(\rho,f_2(\eta;m),\xi')+(1-A)G_2(\rho,f_2(\eta;m),\xi')\}\,\mathrm{d}\xi'\right]. \tag{33}$$

Single pulse Gaussian source

The temporal profile of a single pulse activated for a small time period Δt is

$$f(t) = H(t)-H(t-\Delta t) \tag{34}$$

and the dimensionless form of equation (11) becomes

$$\frac{\partial\theta}{\partial\eta} = -[2\{H(\xi)-H(\xi-\Delta\xi)\}+\delta(\xi)-\delta(\xi-\Delta\xi)]\,\mathrm{e}^{-\mu^2\rho^2}, \quad \text{on} \quad \eta = 0. \tag{35}$$

The temporal profile of the Gaussian source irradiating the surface $\eta = 0$ is rectangular with a width of $\Delta\xi$. In reality, the temporal profile of a pulsed laser does not possess the sharp time discontinuities dictated by a rectangular pulse. The temporally rectangular profile is, however, a useful approximation.

Using the solution procedure previously outlined, the temperature response due to a single pulse Gaussian source is

$$\theta(\rho,\eta,\xi)=\begin{cases}\displaystyle\sum_{m=0}^{\infty}\Bigg[\frac{e^{-\xi}}{2}G_1(\rho,f_1(\eta;m),\xi)H(\xi-f_1(\eta;m))+\int_{\xi'=f_1(\eta;m)}^{\xi}e^{-\xi'}G_1(\rho,f_1(\eta;m),\xi')\,d\xi'\\ \quad+\frac{e^{-\xi}}{2}G_1(\rho,f_2(\eta;m),\xi)H(\xi-f_2(\eta;m))+\int_{\xi'=f_2(\eta;m)}^{\xi}e^{-\xi'}G_1(\rho,f_2(\eta;m),\xi')\,d\xi'\Bigg]\\ -\displaystyle\sum_{m=0}^{\infty}\Bigg[\frac{e^{-\xi^*}}{2}G_1(\rho,f_1(\eta;m),\xi^*)H(\xi^*-f_1(\eta;m))+\int_{\xi'=f_1(\eta;m)}^{\xi'=\xi^*}e^{-\xi'}G_1(\rho,f_1(\eta;m),\xi')\,d\xi'\\ \quad+\frac{e^{-\xi^*}}{2}G_1(\rho,f_2(\eta;m),\xi^*)H(\xi^*-f_2(\eta;m))+\int_{\xi'=f_2(\eta;m)}^{\xi'=\xi^*}e^{-\xi'}G_1(\rho,f_2(\eta;m),\xi')\,d\xi'\Bigg]\end{cases}\tag{36a}$$

where

$$\xi^*=\xi-\Delta\xi.\tag{36b}$$

Again, from the definitions of f_1 and f_2 given by equations (24b) and (24c), the first, second, fifth, and sixth terms in equation (36a) represent the thermal pulses propagating from $\eta=0$ to η_ℓ. The third, fourth, seventh, and eighth terms in equation (36a) represent the thermal pulses reflected from the insulated boundary at $\eta=\eta_\ell$.

Single pulse doughnut source

The temperature response due to a single pulse doughnut source with a temporally rectangular profile is found to be

$$\theta(\rho,\eta,\xi)=\begin{cases}\displaystyle\sum_{m=0}^{\infty}\Bigg[\frac{e^{-\xi}}{2}G_2(\rho,f_1(\eta;m),\xi)H(\xi-f_1(\eta;m))+\int_{\xi'=f_1(\eta;m)}^{\xi}e^{-\xi'}G_2(\rho,f_1(\eta;m),\xi')\,d\xi'\\ \quad+\frac{e^{-\xi}}{2}G_2(\rho,f_2(\eta;m),\xi)H(\xi-f_2(\eta;m))+\int_{\xi'=f_2(\eta;m)}^{\xi}e^{-\xi'}G_2(\rho,f_2(\eta;m),\xi')\,d\xi'\Bigg]\\ -\displaystyle\sum_{m=0}^{\infty}\Bigg[\frac{e^{-\xi^*}}{2}G_2(\rho,f_1(\eta;m),\xi^*)H(\xi^*-f_1(\eta;m))+\int_{\xi'=f_1(\eta;m)}^{\xi'=\xi^*}e^{-\xi'}G_2(\rho,f_1(\eta;m),\xi')\,d\xi'\\ \quad+\frac{e^{-\xi^*}}{2}G_2(\rho,f_2(\eta;m),\xi^*)H(\xi^*-f_2(\eta;m))+\int_{\xi'=f_2(\eta;m)}^{\xi'=\xi^*}e^{-\xi'}G_2(\rho,f_2(\eta;m),\xi')\,d\xi'\Bigg].\end{cases}\tag{37}$$

Single pulse mixed source

The temperature response to a pulsed mixed source is a combination of the temperature profiles given by equations (36a) and (37)

$$\theta(\rho,\eta,\xi)=\begin{cases}\displaystyle\sum_{m=0}^{\infty}\Bigg[\frac{e^{-\xi}}{2}\{AG_1(\rho,f_1(\eta;m),\xi)+(1-A)G_2(\rho,f_1(\eta;m),\xi)\}H(\xi-f_1(\eta;m))\\ \quad+\frac{e^{-\xi}}{2}\{AG_1(\rho,f_2(\eta;m),\xi)+(1-A)G_2(\rho,f_2(\eta;m),\xi)\}H(\xi-f_2(\eta;m))\\ \quad+\displaystyle\int_{\xi'=f_1(\eta;m)}^{\xi}e^{-\xi'}\{AG_1(\rho,f_1(\eta;m),\xi')+(1-A)G_2(\rho,f_1(\eta;m),\xi')\}\,d\xi'\\ \quad+\displaystyle\int_{\xi'=f_2(\eta;m)}^{\xi}e^{-\xi'}\{AG_1(\rho,f_2(\eta;m),\xi')+(1-A)G_2(\rho,f_2(\eta;m),\xi')\}\,d\xi'\Bigg]\\ -\displaystyle\sum_{m=0}^{\infty}\Bigg[\frac{e^{-\xi^*}}{2}\{AG_1(\rho,f_1(\eta;m),\xi^*)+(1-A)G_2(\rho,f_1(\eta;m),\xi^*)\}H(\xi^*-f_1(\eta;m))\\ \quad+\frac{e^{-\xi^*}}{2}\{AG_1(\rho,f_2(\eta;m),\xi^*)+(1-A)G_2(\rho,f_2(\eta;m),\xi^*)\}H(\xi^*-f_2(\eta;m))\\ \quad+\displaystyle\int_{\xi'=f_1(\eta;m)}^{\xi'=\xi^*}e^{-\xi'}\{AG_1(\rho,f_1(\eta;m),\xi')+(1-A)G_2(\rho,f_1(\eta;m),\xi')\}\,d\xi'\\ \quad+\displaystyle\int_{\xi'=f_2(\eta;m)}^{\xi'=\xi^*}e^{-\xi'}\{AG_1(\rho,f_2(\eta;m),\xi')+(1-A)G_2(\rho,f_2(\eta;m),\xi')\}\,d\xi'\Bigg].\end{cases}\tag{38}$$

RESULTS AND DISCUSSION

Numerical computations which model the temperature response due to an axisymmetric heat flux absorbed in the surface plane $\eta = 0$ of a finite medium of width $\eta_\ell = 1$ are displayed in Figs. 2–6. Each figure contains

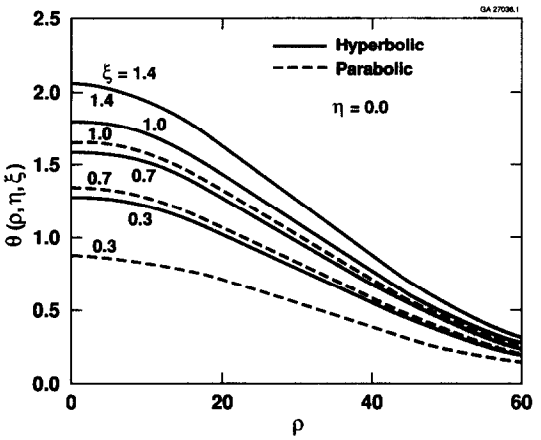

FIG. 2. Temperature distribution at the surface, $\eta = 0$, plotted as a function of the radial position, ρ, for a continuous surface heat flux of Gaussian shape.

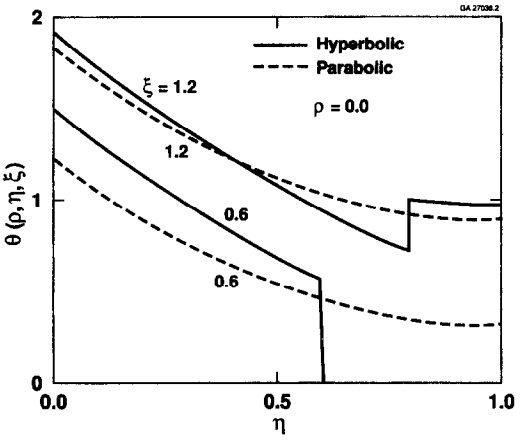

FIG. 3. Variation of center temperature with the axial distance, η, for a continuous surface heat flux of Gaussian shape.

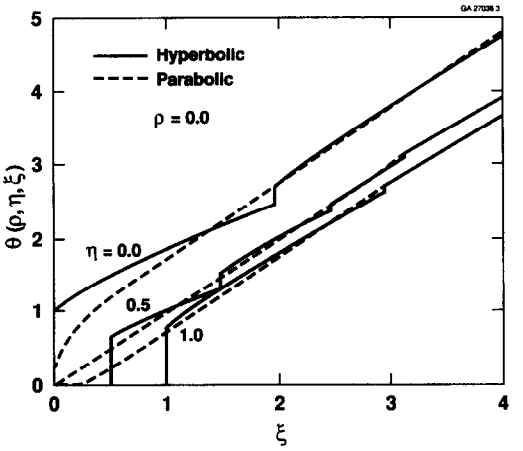

FIG. 4. Variation of center temperature with the time, ξ, for a continuous surface heat flux of Gaussian shape.

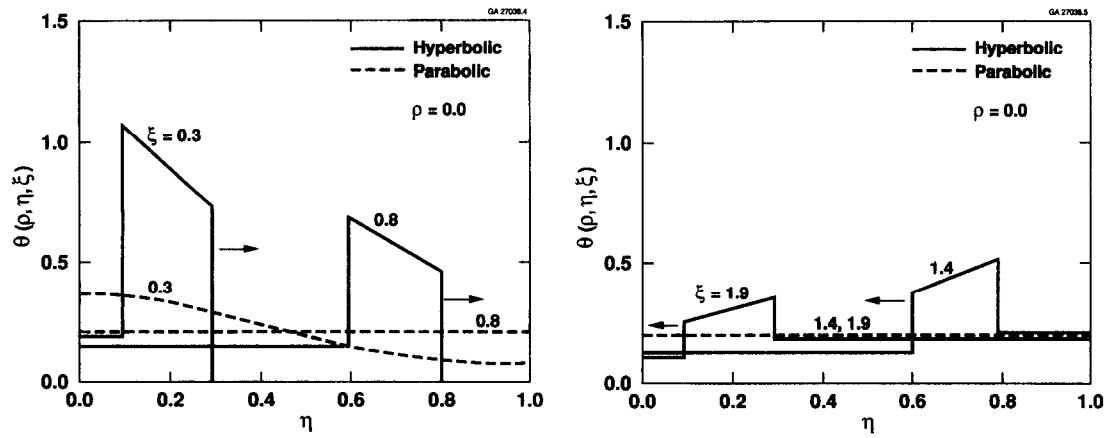

FIG. 5. (a) Variation of center temperature with the axial distance, η, for a pulsed surface heat flux of Gaussian shape. (b) Variation of center temperature with the axial distance, η, for a pulsed surface heat flux of Gaussian shape.

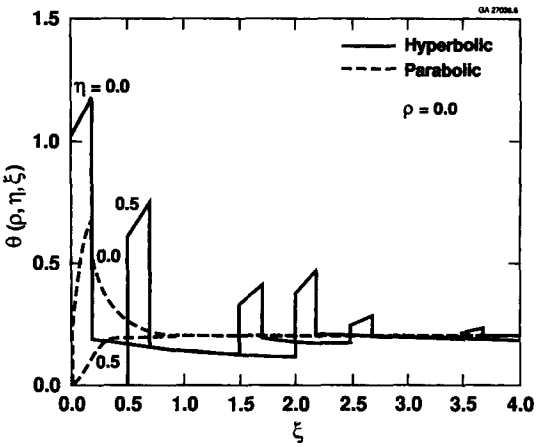

FIG. 6. Variation of center temperature with the time, ξ, for a pulsed surface heat flux of Gaussian shape.

both the hyperbolic and parabolic temperature profiles due to a Gaussian surface source, under the conditions indicated, for purposes of comparison. In Figs. 2–4, a continuous Gaussian source is considered, whereas in Figs. 5 and 6 a rectangular pulse is considered. Similar developments are possible with the doughnut and mixed surface sources although they are not considered here. In each case, ISML numerical integration routines were used to evaluate the temperature distributions. The number of terms used in the summations depended upon the chosen values of ξ and η.

Figure 2 depicts the build-up of temperature on the surface $\eta = 0$ at dimensionless times of $\xi = 0.3, 0.7, 1.0,$ and 1.4. Both the parabolic and hyperbolic surface temperature distributions generally follow a Gaussian profile in that the temperature is maximum at the center $\rho = 0$, and gradually decreases away from the center until the lowest temperatures are reached at the very edge of each profile. The largest differences between the parabolic and hyperbolic solutions occur at the smaller times of $\xi = 0.3$ and 0.7 and at the center of the profile. At these times, the parabolic solution underestimates the surface temperature response when compared with that due to the hyperbolic solution over the range of ρ considered in this figure. At approximately $\xi = 1.4$, the parabolic and hyperbolic solutions are identical and hence the wave nature of heat conduction is not significant. The thermal response of the medium is thus adequately modeled with the classical Fourier heat conduction equation. It should be noted that the hyperbolic model will generally predict higher surface temperatures than the parabolic model since the former requires a finite build-up to the commencement of heat conduction while the latter predicts instantaneous energy propagation.

Figure 3 shows the variation of the temperature along the axis ($\rho = 0$) for dimensionless times of $\xi = 0.6$ and 1.2. Although the net energy content at each time is the same for both models, the distribution of energy in each case is markedly different. At both times, the parabolic model predicts instantaneous energy propagation through the medium since all points of the medium are instantaneously affected by the surface heat source. At $\xi = 0.6$, the hyperbolic model predicts a build-up of temperature at points on the axis which lie within the range $0 \leqslant \eta \leqslant 0.6$ with a severe thermal wavefront at $\eta = 0.6$. Points on the axis which lie in the range $0.6 < \eta \leqslant 1$ have yet to feel the effect of the surface heat source and hence remain at zero temperature. Since the thermal wavefront has not yet reached the insulated boundary at $\eta_\ell = 1$, the limiting solution for the semi-infinite body, given by equation (29a), and the finite body solution, given by equation (28a), predict identical temperature distributions. At $\xi = 1.2$, the thermal wavefront has reflected from the insulated boundary. This is evident from the apparent temperature jump in the hyperbolic profile at $\eta = 0.8$, at which point the thermal wave traveling toward the insulated boundary and that reflected from the insulated boundary overlap resulting in a highly localized temperature increase (a mathematical verification of this fact may be obtained through a comparison of equations (24b) and (24c) at $\eta = 0.8$ and $m = 0$). Such behavior is not evident from the parabolic model which predicts a smooth temperature distribution due to instantaneous energy propagation.

Figure 4 shows the temperature variation with time at three points along the axis. The hyperbolic solution initially predicts a discontinuous jump in temperature at the surface $\eta = 0$. The surface temperature gradually increases up to $\xi = 2.0$ at which time it jumps due to the overlapping of the thermal wave traveling towards the insulated boundary and that reflected from the insulated boundary. For $\xi > 2.0$, there is little difference between the surface temperature predicted by the parabolic and hyperbolic models. At the internal points $\eta = 0.5$ and 1.0, the hyperbolic model predicts that finite times of $\xi = 0.5$ and 1.0, respectively, are required for the commencement of heat conduction. At each of these locations, the temperature again exhibits jumps at discrete times indicating an overlap of thermal waves.

Figure 5(a) shows the variation of temperature along the axis at times $\xi = 0.3$ and 0.8 due to a single surface pulse activated for a period $\Delta\xi = 0.2$. The parabolic temperature profile predicts a smooth build-up of heat transfer in the medium until each point along the axis equilibrates to the same temperature. In contrast to this behavior, the hyperbolic model predicts that the surface pulse generates thermal waves, in the form of temperature pulses of width $\Delta\xi = 0.2$, traveling towards the insulated boundary. During the course of its movement towards the insulated boundary, the thermal wave dissipates energy in its wake and hence the nominal amplitude of the pulse is attenuated with time. Again, the parabolic and hyperbolic models predict dramatically different energy distributions in the medium in response to the surface pulse. Whereas the hyperbolic model predicts highly localized peak energies along the axis, the parabolic model predicts that the peak energies are distributed all along the axis.

Figure 5(b) depicts the temperature pulse considered in Fig. 5(a) after its reflection from the insulated boundary at times $\xi = 1.4$ and 1.9. The amplitude of the reflected pulse is greatly diminished after its reflection from the insulated boundary although the wave nature of heat conduction is still evident. With increasing time, differences between the hyperbolic and parabolic models greatly diminish.

Figure 6 shows the variation of the axial temperature with time at two points on the axis due to a surface pulse activated for a period $\Delta\xi = 0.2$. At the surface, the parabolic solution predicts a sharp but smooth rise in temperature at initial time, to a maximum temperature at $\xi = 0.2$, at which time the surface pulse is deactivated. The temperature then gradually decreases to a nearly constant value. On the other hand, the hyperbolic model predicts that a severe initial temperature is sustained at the surface of the body during the time when the pulse is activated. After the pulse is deactivated, the temperature abruptly drops. A similar behavior is found at the midpoint of the axis, $\eta = 0.5$, although the amplitude of the pulse is significantly attenuated from that at the surface. An interesting effect which is due to reflection of the surface temperature pulse from the boundaries is evident from the additional pulses centered at times $\xi = 1.6$, 2.1, 2.6, and 3.6. The pulse centered at $\xi = 2.1$ represents the jump in surface temperature due to reflection of the surface pulse from the insulated boundary. Similarly, the pulse centered at $\xi = 1.6$ represents the jump in temperature at $\eta = 0.5$ due to arrival of the reflected pulse at that point. The pulse centered at $\xi = 2.6$ represents the jump in temperature at $\eta = 0.5$ due to partial reflection of the pulse from the surface, and finally, an additional reflection at $\eta = 0.5$ is evident at $\xi = 3.6$ from the insulated surface. In each case the amplitude of the pulse is greatly attenuated since the pulse dissipates energy through the medium. At later times the parabolic model predicts little change, if any, in the temperature at the surface and midpoint of the axis since energy from the surface pulse is instantaneously distributed in the medium.

CONCLUSIONS

The transient temperature distribution in a two-dimensional isotropic medium with one surface subjected to an axisymmetric heat source and the other surface insulated has been determined using the hyperbolic heat conduction model. Gaussian and doughnut profiles, which are either temporally continuous or rectangular pulses, were chosen since they adequately model the output from many laser sources. A comparison of temperature distributions resulting from the hyperbolic and parabolic models reveals that, for extremely short times, the parabolic model significantly underestimates the surface temperature. The hyperbolic model predicts a severe thermal wavefront which dissipates energy in its wake as it travels through the medium. Due to the overlapping of reflected thermal waves from the two boundaries, the hyperbolic temperature profile exhibits jumps along the axis of the material. A comparison of the relative importance of the parabolic and hyperbolic models for a metal exposed to three regimes of rectangular pulse width revealed that the hyperbolic model becomes significant for pulse widths of the order of 10^{-10} s if the thermal field due to an accompanying dilatational wave is neglected.

In the present analysis, the thermophysical properties are assumed to be constants so that analytic solutions to the problem may be obtained. In reality, the material properties vary with temperature; but for such cases the problem should be solved by purely numerical approaches. In situations involving high surface temperatures, the inclusion of the fourth power temperature law in the boundary condition for heat flux also results in a non-linear problem which should be solved numerically.

Acknowledgments—This work was supported in part by the Precision Engineering Program at Alcoa Laboratories. One of the authors (W. S. Kim) wishes to acknowledge the financial support of Alcoa Laboratories during his tenure as a postdoctoral research associate in the Mechanical and Aerospace Engineering Department at North Carolina State University. The authors wish to thank Dr Owen Richmond of Alcoa Laboratories for his continued support of this work.

REFERENCES

1. J. C. Maxwell, On the dynamical theory of gases, *Phil. Trans. R. Soc. London* **157**, 49–88 (1867).
2. J. P. Brazel and E. J. Nolan, Non-Fourier effects in the transmission of heat, *Proc. Sixth Conf. on Thermal Conductivity*, U.S. Air Force Materials Laboratory, Dayton, Ohio, pp. 237–254 (1966).

3. J. Gembarovic and V. Majermik, Determination of thermal parameters of relaxation materials, *Int. J. Heat Mass Transfer* **30,** 199–201 (1987).
4. W. Kaminsky, Hyperbolic heat conduction equation for materials with a nonhomogeneous inner structure, *ASME J. Heat Transfer* **112,** 555–560 (1990).
5. S. Simons, On the differential equation for heat conduction, *Transp. Theory Statist. Phys.* **2,** 117–128 (1972).
6. M. Chester, Second sound in solids, *Phys. Rev.* **131,** 2013–2015 (1963).
7. M. von Allen, Coupling of beam energy to solids, *Proc. Symp. on Laser and Electron Beam Processing of Materials.* Materials Research Society, pp. 6–19 (1979).
8. G. F. Carey and M. Tsai, Hyperbolic heat transfer with reflection, *Numer. Heat Transfer* **5,** 309–327 (1982).
9. M. N. Özisik and B. Vick, Propagation and reflection of thermal waves in a finite medium, *Int. J. Heat Mass Transfer* **27,** 1845–1854 (1984).
10. J. I. Frankel, B. Vick and M. N. Özisik, Flux formulation of hyperbolic heat conduction, *J. Appl. Phys.* **58,** 3340–3345 (1985).
11. D. S. Chandrasekaraiah, Thermoelasticity with second sound: a review, *Appl. Mech. Rev.* **39,** 355–376 (1989).
12. V. G. Gregson and B. A. Sanders, A physical model of laser heat treatment, *Proc. 1974 Electro-Optic Systems Design Conf.*, Industrial and Scientific Management, pp. 237–243 (1974).
13. Y. Arata and I. Miyamoto, Some fundamental properties of high power laser beam as a heat source, *Trans. Japan Welding Soc.* **3,** 152–169 (1972).
14. K. Brugger, Exact solutions for the temperature rise in a laser-heated slab, *J. Appl. Phys.* **43,** 577–583 (1972).
15. T. P. Lin, Estimation of temperature rise in electron beam heating of thin films, *IBM J. Res. Dev.* **11,** 527–536 (1967).
16. J. L. Deming, L. C. Tao and J. H. Weber, Numerical solution of disk source problems, *A.I.Ch.E. Jl* **13,** 1214–1216 (1967).
17. A. Bloyce and T. Bell, Laser surface engineering. In *Industrial Laser Annual Handbook* (Edited by D. Belforte and M. Levitt), pp. 61–68. PennWell, Tulsa, Oklahoma (1988).
18. M. Sparks, Theory of laser heating of solids: metals, *J. Appl. Phys.* **47,** 837–849 (1976).
19. W. Walter, Change in reflectivity of metals under intense laser radiation, Final Technical Report Microwave Research Inst., Polytechnic Inst. New York, AFOSR-TR-81-0567 (1980).
20. G. C. Lim, Laser beam quality. In *Industrial Laser Annual Handbook* (Edited by D. Belforte and M. Levitt), pp. 96–116. PennWell, Tulsa, Oklahoma (1989).
21. M. N. Özisik, *Heat Conduction*, Chaps 7 and 13. Wiley, New York (1980).
22. G. N. Watson, *A Treatise on the Theory of Bessel Functions*, 2nd Edn, p. 394. Cambridge University Press, London (1966).
23. M. J. Maurer and H. A. Thompson, Non-Fourier effects at high heat flux, *ASME J. Heat Transfer* **95,** 284–286 (1973).
24. J. Hecht, *The Laser Guidebook*, pp. 284–302. McGraw-Hill, New York (1986).
25. W. Koechner, *Solid State Laser Engineering*, 2nd Edn, Chap. 8. Springer, New York (1988).

APPENDIX A. WHEN IS HYPERBOLIC HEAT CONDUCTION IMPORTANT DURING PULSED LASER IRRADIATION OF METALS?

The following developments neglect the dilatational or shock wave which may accompany impulsive heating since the solution to this coupled problem is beyond the scope of this paper. It should be kept in mind that the deformation of the material in these situations can make a significant contribution to the thermal field [11].

The parabolic or Fourier heat conduction equation is given by

$$\nabla^2 T = \frac{1}{\alpha}\frac{\partial T}{\partial t}. \tag{A1}$$

The hyperbolic heat conduction equation is given in terms of temperature by equation (3) of the paper

$$\nabla^2 T = \frac{1}{c^2}\frac{\partial^2 T}{\partial t^2} + \frac{1}{\alpha}\frac{\partial T}{\partial t} \tag{3}$$

and in terms of heat flux $\mathbf{q}$, by [10]

$$\nabla[\nabla \cdot \mathbf{q}] = \frac{1}{c^2}\frac{\partial^2 \mathbf{q}}{\partial t^2} + \frac{1}{\alpha}\frac{\partial \mathbf{q}}{\partial t}. \tag{A2}$$

In order to determine the relative importance of the hyperbolic and parabolic models, it is necessary to compare the two terms on the right-hand side of either equation (3) or equation (A2). For a material to exhibit wave nature of heat conduction, equation (3) requires that

$$\frac{1}{c^2}\frac{\partial^2 T}{\partial t^2} \gg \frac{1}{\alpha}\frac{\partial T}{\partial t} \tag{A3}$$

and equation (A2) requires that

$$\frac{1}{c^2}\frac{\partial^2 q}{\partial t^2} \gg \frac{1}{\alpha}\frac{\partial q}{\partial t} \tag{A4}$$

where we have dropped the bold face vectorial notation in equation (A2). Equation (A3) may be written as

$$\frac{\partial \Gamma}{\partial t} \gg \frac{c^2}{\alpha}\Gamma \tag{A5}$$

where

$$\Gamma \equiv \frac{\partial T}{\partial t}. \tag{A6}$$

When equation (A5) is integrated, we find

$$\Gamma \equiv \frac{\partial T}{\partial t} \gg C_1 e^{(c^2/\alpha)\Delta t} (= C_1 e^{\Delta t/\tau}) \tag{A7}$$

where C_1 is an unknown constant. Similarly, integration of equation (A4) yields

$$\frac{\partial q}{\partial t} \gg C_2 e^{(c^2/\alpha)\Delta t} (= C_2 e^{\Delta t/\tau}) \tag{A8}$$

where C_2 is another unknown constant. If either of the conditions given by equation (A7) or (A8) is satisfied, then the wave nature of heat conduction is important.

For many metals, the thermal diffusivity is approximately 10^{-5} m^2 s^{-1} during the initial stages of laser irradiation and the relaxation time is of the order of 10^{-11} s [3]. According to Maurer and Thompson [23], the wave nature of heat conduction is appropriate when the surface heat flux is equal to or greater than 10^{11} W m^{-2}. Therefore, the thermal wave speed is of the order of

$$c = \sqrt{\left(\frac{\alpha}{\tau}\right)} \approx 1000 \text{ m s}^{-1} \tag{A9}$$

and the limiting heat flux is taken to be

$$\Delta q_\ell = 10^{11} \text{ W m}^{-2}. \tag{A10}$$

A comparison of the relative importance of the diffusive (Fourier) and wave (non-Fourier) models for a metal irradiated with three ranges of rectangular pulse width, along with potential sources may be found in Table A1. According to the criterion established by equation (A8), the Fourier heat conduction equation adequately models heat transfer due to nanosecond pulses (assuming the unknown constant multiplier to have a value of one). For pulse widths less than a nanosecond, heat conduction changes from a diffusive behavior to a dissipative wave behavior over the short times of interest. Additional background on the solid state lasers mentioned in Table A1 may be found in Hecht [24] or Koechner [25].

APPENDIX B. VOLUMETRIC SOURCE FORMULATION

Many heat transfer problems associated with laser irradiation can be written in terms of a volumetric heat source term which includes the effect of the attenuation of absorbed energy with depth beneath the surface. In terms of a volumetric heat source, equation (7) may be re-written as

$$\frac{\partial^2 T}{\partial r^2} + \frac{1}{r}\frac{\partial T}{\partial r} + \frac{\partial^2 T}{\partial z^2} + \frac{\gamma q_0}{k}\left\{f(t) + \tau \frac{df(t)}{dt}\right\} e^{-(r^2/d^2 + \gamma z)} = \frac{1}{\alpha}\frac{\partial T}{\partial t} + \frac{1}{c^2}\frac{\partial^2 T}{\partial t^2} \tag{B1}$$

where γ is the attenuation coefficient and a Gaussian profile is assumed. Equation (B1) indicates that the energy absorbed in the medium is exponentially damped through the medium thickness. Also, the inclusion of a time derivative on $f(t)$ in the source term is required by the hyperbolic constitutive law (equation (2)). Since the attenuation coefficient is typically of the order of 10^5–10^6 cm^{-1} for most metals [19], the absorbed energy can be regarded as a surface heat source. Therefore, the z-dependence in the source becomes

$$\lim_{\gamma \to \infty} \gamma e^{-\gamma z} = \delta(z) \tag{B2}$$

where $\delta(z)$ is the delta function of argument z. The solution of equation (B1), subject to

Table A1. Regimes of diffusive and dissipative wave propagation models

Pulse duration (s)	$\Delta q_\ell/\Delta t$ (W m^{-2} s^{-1})	$e^{\Delta t/\tau}$	Dominant heat conduction mechanism	Representative pulse source
10^{-8}–10^{-9}	10^{19}–10^{20}	10^{440}–10^{44}	Diffusion	Ruby laser Q-Switched Nd : YAG laser (with or without harmonic generation) Excimer laser Nd : glass lasers (with or without harmonic generation) Cavity-dumped Nd : YAG laser
10^{-9}–10^{-10}	10^{20}–10^{21}	10^{44}–10^{5}	Diffusion–dissipative wave propagation	Modelocked Nd : YAG laser Cavity-dumped Nd : YAG laser Q-Switched, modelocked Nd : YAG laser Cavity-dumped, modelocked Nd : YAG laser
10^{-10}–10^{-11}	10^{21}–10^{22}	10^{5}–10^{1}	Dissipative wave propagation	Modelocked Nd : YAG laser Q-Switched, modelocked Nd : YAG laser Cavity-dumped, modelocked Nd : YAG laser

For a metal : $\tau = 10^{-11}$ s ; $\alpha = 10^{-5}$ m^2 s^{-1} ; $c = 1000$ m s^{-1} ; $\Delta q_\ell = 10^{11}$ W m^{-2}.

$$\frac{\partial T}{\partial z} = 0, \quad \text{at} \quad z = 0 \tag{B3}$$

and equations (9a), (9b) and (12a)–(12c) is thus identical to the solution of equation (7) subject to equations (9a), (9b), (11) (with $A = 1$) and (12a)–(12c).

APPENDIX C. FOURIER HEAT CONDUCTION SOLUTIONS

Continuous mixed source

$$\theta(\rho,\eta,\xi) = \sqrt{\left(\frac{2}{\pi}\right)} \sum_{m=0}^{\infty} \left[\int_{\xi'=0}^{\xi} \{AG_3(\rho, f_1(\eta;m), \xi') + (1-A)G_4(\rho, f_1(\eta;m), \xi')\} \frac{d\xi'}{\sqrt{\xi'(1+2\mu^2\xi')}} \right.$$
$$\left. + \int_{\xi'=0}^{\xi} \{AG_3(\rho, f_2(\eta;m), \xi') + (1-A)G_4(\rho, f_2(\eta;m), \xi')\} \frac{d\xi'}{\sqrt{\xi'(1+2\mu^2\xi')}} \right] \tag{C1}$$

where

$$G_3(\rho, f_i(\eta;m), \xi) = \exp\left\{ -\left(\frac{f_i^2(\eta;m)}{2\xi} + \frac{\mu^2\rho^2}{1+2\mu^2\xi} \right) \right\} \tag{C2}$$

$$G_4(\rho, f_i(\eta;m), \xi) = \left\{ 1 - \frac{1}{1+2\mu^2\xi} \left(1 - \frac{\mu^2\rho^2}{1+2\mu^2\xi} \right) \right\} G_3(\rho, f_i(\eta;m), \xi). \tag{C3}$$

Continuous Gaussian source. Set $A = 1$ in equation (C1).
Continuous doughnut source. Set $A = 0$ in equation (C1).

Single pulse mixed source

$$\theta(\rho,\eta,\xi) = \sqrt{\left(\frac{2}{\pi}\right)} \sum_{m=0}^{\infty} \left[\begin{array}{l} \displaystyle\int_{\xi'=0}^{\xi} \{AG_3(\rho, f_1(\eta;m), \xi') + (1-A)G_4(\rho, f_1(\eta;m), \xi')\} \frac{d\xi'}{\sqrt{\xi'(1+2\mu^2\xi')}} \\ \displaystyle\int_{\xi'=0}^{\xi} \{AG_3(\rho, f_2(\eta;m), \xi') + (1-A)G_4(\rho, f_2(\eta;m), \xi')\} \frac{d\xi'}{\sqrt{\xi'(1+2\mu^2\xi')}} \\ \displaystyle -\int_{\xi'=0}^{\xi'=\xi^*} \{AG_3(\rho, f_1(\eta;m), \xi') + (1-A)G_4(\rho, f_1(\eta;m), \xi')\} \frac{d\xi'}{\sqrt{\xi'(1+2\mu^2\xi')}} \\ \displaystyle -\int_{\xi'=0}^{\xi'=\xi^*} \{AG_3(\rho, f_2(\eta;m), \xi') + (1-A)G_4(\rho, f_2(\eta;m), \xi')\} \frac{d\xi'}{\sqrt{\xi'(1+2\mu^2\xi')}} \end{array} \right]. \tag{C4}$$

Single pulse Gaussian source. Set $A = 1$ in equation (C4).
Single pulse doughnut source. Set $A = 0$ in equation (C4).

PROPAGATION DANS UN MILIEU FINI ET REFLEXION D'ONDES THERMIQUES DUES A DES SOURCES AXISYMETRIQUES EN SURFACE

Résumé—Pour des situations de temps extrèmement court après l'origine du transitoire ou de flux thermique très élevé, la théorie classique de diffusion de la chaleur n'est pas valable parce que la nature ondulatoire domine dans le transport d'lénergie. On considère ici la réponse hyperbolique dans un milieu fini isotrope avec une surface isolée et l'autre surface irradiée avec un flux thermique axialement symétrique. Le profil spatial du flux est choisi soit Gaussien, soit en forme de beignet, soit en combinaison des deux formes. Le profil temporel est soit continu, soit un créneau. Le choix de ces profils est basé sur le fait qu'ils approchent la sortie des sources laser. Les calculs pour une source Gaussienne révèlent l'existence d'un front d'onde thermique sévère qui se propage à travers le milieu, dissipant l'énergie dans son sillage par réflexion aux frontières. On discute aussi l'importance relative des modèles de conduction parabolique et hyperbolique pour un métal exposé à trois domaines de durée de créneau rectangulaire.

AUSBREITUNG UND REFLEXION THERMISCHER WELLEN IN EINEM ENDLICHEN MEDIUM MIT ACHSENSYMMETRISCH VERTEILTEN QUELLEN AN DER OBERFLÄCHE

Zusammenfassung—Bei Betrachtungen, die sich auf sehr kurze Zeiten nach der Auslösung transienter Vorgänge oder auf sehr große Wärmestromdichten beziehen, versagt die klassische Theorie der Wärmeleitung durch Diffusion, da die Wellennatur des thermischen Energietransportes dominiert. In der vorliegenden Arbeit wird das hyperbolische Temperaturverhalten in einem endlichen isotropen Medium betrachtet. Das Medium besitzt eine adiabate Oberfläche und wird auf der anderen Oberfläche mit einem achsensymmetrischen Wärmestrom beaufschlagt. Das räumliche Profil der Wärmestromdichte wird entsprechend einer Gauß-Verteilung, oder wulstförmig oder als eine Kombination aus beiden gewählt. Das zeitliche Profil ist entweder kontinuierlich oder es entspricht einem Rechteckimpuls. Die Wahl der Profile wird unter der Annahme getroffen, daß sie ungefähr der Abstrahlung von üblichen Laser-Quellen entsprechen. Berechnungen für die Gauß-Quelle offenbaren die Existenz von scharf abgegrenzten thermischen Wellenfronten, welche durch das Medium wandern und dabei auf ihrem Weg bis zur Reflexion Energie im Medium dissipieren. Zusätzlich wird die relative Bedeutung der parabolischen und hyperbolischen Modelle für die Wärmeleitung in einem metallischen Körper diskutiert, welcher drei unterschiedlichen Typen von Rechteckimpulsen ausgesetzt wird.

РАСПРОСТРАНЕНИЕ И ОТРАЖЕНИЕ ТЕПЛОВЫХ ВОЛН В ОГРАНИЧЕННОЙ СРЕДЕ ЗА СЧЕТ РАСПОЛОЖЕННЫХ НА ПОВЕРХНОСТИ ОСЕСИММЕТРИЧНЫХ ИСТОЧНИКОВ

Аннотация—Для очень малых промехутков времени после возникновения нестационарного состояния классическая диффузионная теория теплопроводности нарушается, поскольку преобладает волновой характер теплопереноса. Исследуется гиперболический тепловой отклик в ограниченной изотропной среде, одна поверхность которой изолирована, а на другой имеет место осесимметричный тепловой поток. Выбранный пространственный профиль теплового потока является гауссовским или тороидальным, или же их комбинацией. Временная зависимость потока монотонна или представляет собой прямоугольный импульс. Выбор указанных профилей основан на допущении, что они аппроксимируют излучение некоторых лазерных источников. Расчеты для гауссовского источника указывают на существование жесткого волнового фронта, распространяющегося в среде и рассеивающего энергию в следе при отражении на границах. Обсуждается также применимость параболической и гиперболической моделей теплопроводности в случае воздействия на металл прямоугольного испульса с различной длительностью.